Research Article

Jaruwan Thepsiri, Sasiporn Audtarat, and Thananchai Dasri*

Green synthesis of silver nanoparticles using *Ageratum conyzoides* for activated carbon compositing to prepare antimicrobial cotton fabric

https://doi.org/10.1515/ntrev-2025-0181
received December 29, 2024; accepted May 18, 2025

Abstract: Wearing socks or shoes for an extended time can result in the growth of microorganisms and associated foot odor, which affects foot hygiene. Therefore, the development of an antimicrobial cloth layer is needed to prevent these odors. In this work, silver nanoparticles (AgNPs) are prepared using *Ageratum conyzoides* leaf extract mixed with hemp-activated carbon (HAC) (AgNPs-HAC) coated on cotton fabric (CF) surfaces. CFs were modified using a plasma technique to improve AgNP adherence (PCFs) (PCFs@HAC-AgNPs). The prepared AgNPs and sheets of PCFs@HAC-AgNPs were evaluated for the formation of AgNPs by ultraviolet–visible spectroscopy, surface morphology and particle size by transmission electron microscopy and field emission scanning electron microscopy, and crystallinity by X-ray diffraction. The result showed that AgNPs had a crystalline structure and uniform distribution on PCFs@HAC-AgNP sheets. The antimicrobial activity of PCFs@HAC-AgNP sheets was tested against *Staphylococcus aureus* and *Bacillus subtilis* bacteria that cause foot odor. All sheets showed strong antibacterial activity against both bacteria. Additionally, the sheets were evaluated for antimicrobial durability after washing. Although the sheets underwent numerous washing cycles, their antibacterial performance was retained with low environmental impact. These results indicate that PCFs@HAC-AgNP sheets can be used in the development of odor-reducing materials for shoes that can be laundered and reused.

*** Corresponding author: Thananchai Dasri,** Faculty of Interdisciplinary Studies, Khon Kaen University, Nong Khai Campus, Nong Khai, 43000, Thailand, e-mail: thananchai@kku.ac.th
Jaruwan Thepsiri, Sasiporn Audtarat: Faculty of Interdisciplinary Studies, Khon Kaen University, Nong Khai Campus, Nong Khai, 43000, Thailand

Keywords: silver nanoparticles, cotton fabrics, activated carbon, plasma treatment, antimicrobial activity

1 Introduction

Foot odor is an unpleasant problem, especially for people who wear socks or shoes for extended periods. The origin of foot odor is sweat from the feet. Foot sweating enables bacterial growth, which breaks down the chemical components of the sweat, resulting in foot odor (foot malodor). In some cases, it can become severe enough to develop into a condition known as pitted keratolysis [1,2]. There have been reports of bacteria responsible for causing foot odor, including *Micrococcus sedentarius*, *Bacillus subtilis*, *Staphylococcus epidermidis*, *Staphylococcus aureus*, *Propionibacterium acnes*, and *Brevibacterium epidermidis*. These bacteria reside on the human skin and break down amino acids, such as leucine and methionine, which are components of sweat, leading to the production of compounds that have a strong odor, such as methanethiol, propionic acid, and isovaleric acid [1–4]. There are ways of reducing foot odors, such as always keeping one's feet dry, using an odor suppressant spray, or inhibiting the growth of odor-causing bacteria with antimicrobial products [5]. There is increased interest in odor-preventing products made from cotton fabric (CF) because these materials have excellent liquid absorption properties, good breathability, and softness, affording comfort to the wearer. However, CFs are a natural fiber that can collect moisture and enable bacterial growth, resulting in malodor. Also, some bacteria are harmful to human health [6]. Therefore, optimizing the bacterial inhibition of CFs by compositing them with metal nanoparticles is a viable approach to address these problems. Compositing materials involves combining two or more materials to achieve a material with overall enhanced properties. As a result, commercially available modified tissue products are now in high

demand in medical fields and markets [7]. Metal nanoparticles, such as Ag, Cu, Au, and TiO_2, have antibacterial properties. However, silver nanoparticles (AgNPs) are most commonly used due to their unique biological, optical, and physicochemical properties [8]. AgNPs (Ag^0) exhibit high antimicrobial efficacy and significantly inhibit the growth of various Gram-negative and Gram-positive bacterial species [9,10]. Earlier studies reported on effective synthesis techniques for AgNPs, including chemical, biological, and physical methods. A biological process was utilized in the current work because it does not require toxic chemicals and is environmentally friendly. *Ageratum conyzoides* L. is a weed species in the Asteraceae family [11]. It contains several phytochemicals, including alkaloids, flavonoids, chromenes, benzofurans, and terpenoids, which can reduce silver ions (Ag^+) to metallic Ag (Ag^0) [12,13]. AgNPs are widely employed in medicine, the textile industry, the environment, and agriculture, among other areas. Owing to their bacterial-inhibitory properties, they are incorporated into fabrics, textiles, clothing, and medical devices to inactivate bacteria and reduce unwanted odors [14]. AgNPs can be composited with activated carbon (AC) for enhanced odor absorption capabilities. AC is produced through an activation process of carbon black. It has a high porosity and a surface area of approximately 500–2,000 m^2/g, enabling a high absorption capacity [15]. The current study involved coating hemp-activated carbon (HAC)-AgNP composites on textiles. Consequently, the adhesion of nanometals onto textiles is a significant concern. When textiles come into contact with skin or liquids, these nanometals may leach from the textiles, especially when their concentrations are high [16]. Various methods have been proposed to reduce the impact of leaching using adjunct materials or by chemically or physically altering textile materials using ultrasound, ultraviolet (UV) radiation, and microwaves, among other approaches [17]. In the current work, plasma treatment was done to improve the adhesion of HAC-AgNPs onto fabric surfaces because it offers an eco-friendly method for modifying cotton surfaces without altering their internal properties [18].

The current work aims to synthesize AgNPs using an extract from the leaves of *A. conyzoides*, employing it as a reducing agent. Synthesized AgNPs were then composited with AC prepared from hemp hurd and coated onto CFs that had undergone surface modification with plasma (PCFs) to enhance the adhesion of AgNPs and AC onto the fabric. Finally, the antimicrobial activity of PCFs@HAC-AgNPs samples was evaluated against bacteria causing foot odor, *S. aureus* and *B. subtilis*, and samples were assessed for antimicrobial durability after washing. Additionally, samples were tested by quantitative techniques as a novelty. The resulting materials were characterized using UV–visible (UV–vis) spectroscopy, diffuse reflectance spectroscopy (DRS), field emission scanning electron microscopy (FE-SEM), transmission electron microscopy (TEM), X-ray diffraction (XRD) analysis, and Fourier transform infrared (FT-IR) spectroscopy.

2 Materials and methods

2.1 Chemicals and materials

Healthy, fresh leaves of *A. conyzoides* plants were collected from agricultural areas in Nong Khai Province, Thailand. CFs were sourced from textile markets in Nong Khai Province, Thailand. The hemp stalk core material was received from Khon Kaen University, Thailand. Silver nitrate ($AgNO_3$) was purchased from RCI Labscan, Ltd. (Bangkok, Thailand). Polyvinylalcohol (PVA) was procured from Chem Supply Pty, Ltd. (Gillman, Australia). *N*-Methyl-2-pyrrolidone (NMP) was acquired from WINNEX (Thailand) Co., Ltd. (Bangkok, Thailand). Nutrient broth (NB) and nutrient agar (NA) were obtained from HiMedia Laboratories Pvt., Ltd. (Mumbai, India). *S. aureus* and *B. subtilis* strains were obtained from the Biosafety Level II Laboratory (BSL2), Faculty of Interdisciplinary Studies, Khon Kaen University, Thailand.

2.2 Preparation of *A. conyzoides* leaf extract (ACLE)

Fresh *A. conyzoides* leaves were cleaned with deionized water, dried at room temperature, and ground into a coarse powder using a mortar and pestle. Afterward, 4.0 g of the *A. conyzoides* powder sample was mixed with 100 mL of distilled water, heated at 55°C for 15 min in a water bath, and cooled to room temperature. Then, the resulting leaf extract was filtered through Whatman No. 1 filter paper and further used to synthesize AgNPs.

2.3 Green synthesis optimization of AgNPs using ACLE

2.3.1 The effects of various concentrations of silver nitrate ($AgNO_3$)

One milliliter of ACLE was added to 9 mL of $AgNO_3$ at 4, 6, 8, 10, and 12 mM concentrations followed by heating for 10 min at 60°C in a water bath. Then, the mixed solution

was incubated under dark conditions for 2 h at 30°C. The absorbance spectra of the solutions were measured using UV–vis spectroscopy at 300–700 nm wavelengths. The 10 mM $AgNO_3$ concentration showed high AgNP synthesis. Therefore, this $AgNO_3$ concentration was used in further studies.

2.3.2 The effects of various ACLE volumes

ACLE volumes of 0.6, 0.8, 1, 1.2, and 1.4 mL were made up to 10 mL using 10 mM $AgNO_3$ and heated for 10 min at 60°C in a water bath. Then, the mixed solution was incubated under dark conditions for 2 h at 30°C. The absorbance spectra of the solutions were subjected to UV–vis spectroscopy. A 10 mM solution of $AgNO_3$ mixed with 1.2 mL ACLE showed the highest synthesis of AgNPs. Therefore, this solution was selected for use in further studies.

2.3.3 Temperature effects

An 8.8 mL solution of 10 mM $AgNO_3$ mixed with 1.2 mL ACLE was heated for 10 min at various temperatures, 50, 55, 60, and 65°C, in a water bath. Then, the mixed solutions were incubated under dark conditions for 2 h at 30°C. The absorbance spectra of the solutions were measured with UV–vis spectroscopy. Mixtures heated at 60°C showed high synthesis of AgNPs and this temperature was used in further studies.

2.3.4 The effects of reaction time

A 1.2 mL aliquot of ACLE was added to 8.8 mL of 10 mM $AgNO_3$ and heated at 60°C in a water bath for various times, 0, 1, 4, 7, 10, and 13 min. Then, the mixed solutions were incubated under dark conditions for 2 h at 30°C. The absorbance spectra of the solutions were detected using UV–vis spectroscopy. A 1 min synthesis for AgNPs was most suitable. After that, the colloidal solution of AgNPs was centrifuged at 12,000 rpm for 5 min and dried at 60°C in an oven. Finally, the AgNPs were characterized. An AgNP synthesis procedure using ACLE is shown in Figure 1.

2.4 Surface modification of CFs

In the current work, the surfaces of CFs were improved using plasma treatment. This treatment was performed at atmospheric pressure with a 100 W discharge at an 80 kHz frequency. The process was conducted using cylindrical nozzles with several holes having an active area of

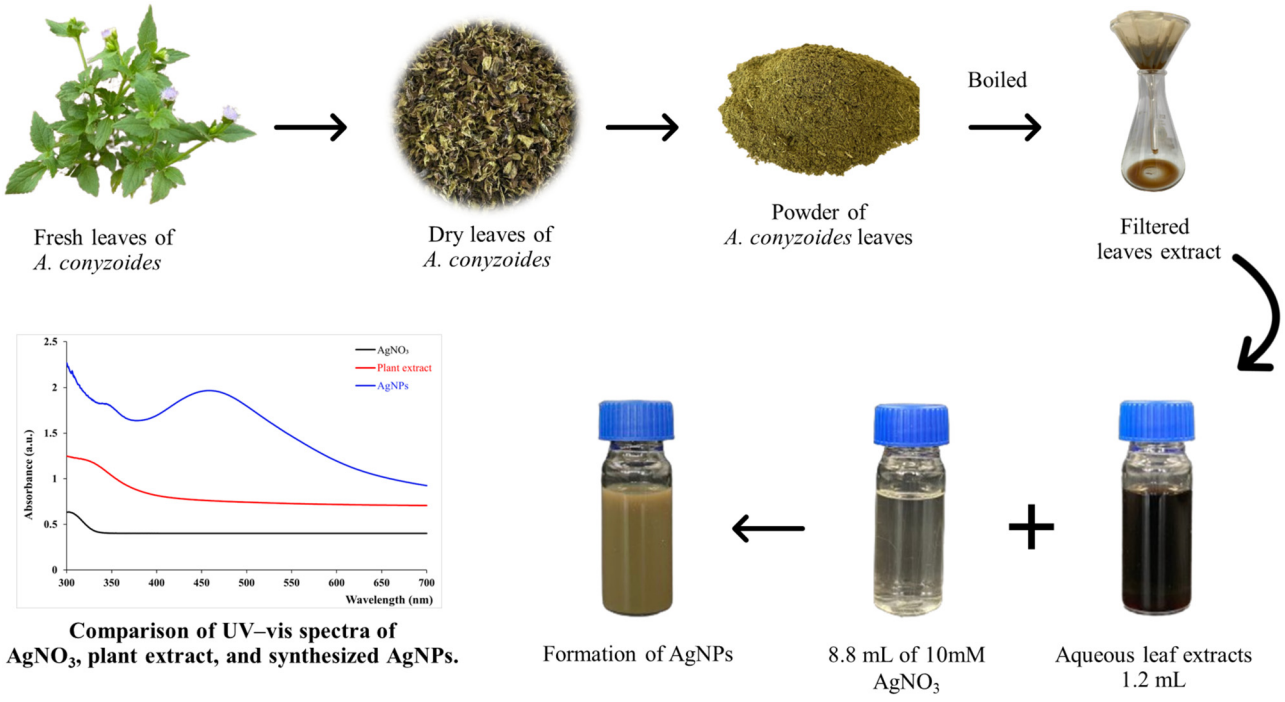

Figure 1: Schematic illustration of the green synthesis of AgNPs using *A. conyzoides*.

200 mm by 120 mm, positioned vertically over the CF substrate. Additionally, CFs were argon plasma treated at a flow rate of 2 l/min over 8 cycles, with a scanning speed of 1 mm/s and a 2 mm nozzle-to-substrate distance [19].

2.5 Preparation of HAC

To produce the HAC, dried hemp hurd was first carbonized by pyrolysis at 400°C for 60 min. Then, a physical activation was done by heating hemp carbon at 850°C for 30 min with water steam addition. Afterward, the samples were naturally cooled and hermetically packaged for future use [20].

2.6 Preparation of AgNPs-HAC coated on PCFs (PCFs@HAC-AgNPs)

Binder concentrations of 5% (w/v) were prepared by mixing PVA with NMP and continuously stirring at 80°C for 1 h [19]. Then, mixtures of 0.01 g of HAC with different concentrations of AgNPs, 62.5, 125, 250, 500, and 1,000 µg/mL, were sonicated for 30 min. After the mixture was dispersed, it was coated on the PCFs using a dip method, immersing the PCFs into the mixture for 30 min followed by drying. Afterward, the antibacterial properties and wash fastness of PCFs@HAC-AgNPs sheets were further investigated.

2.7 Characterization

AgNP formation was monitored with UV–vis spectral analysis using a Shimadzu UV-1900i UV–vis spectrophotometer, DRS. Absorbance was measured at 300–700 nm wavelengths. AgNP morphology and particle size were examined using TEM (FEI model TECNAI G2 20). The morphology and adhesion of HAC and AgNPs coated on PCFs were verified using FE-SEM with a TESCAN model MIRA instrument. The crystallinity of synthesized AgNPs was confirmed using XRD analysis scanned over a 2θ range from 25 to 80° with a step size of 0.2°. Sample functional groups were detected using FT-IR spectroscopy (Bruker model Invenio-s).

2.8 Wash fastness tests of PCFs@HAC-AgNP sheets

The PCFs@HAC-AgNP samples were washed with 1 g/L of ion-free detergent in an ultrasonic cleaner over 1 and 3 cycles. One-cycle washing is equivalent to five cycles at home. These samples were dried and evaluated for their antimicrobial activity.

2.9 Evaluation of the retention of AgNPs coated in PCFs

A method proposed by Durán *et al.* [21] with modifications was employed to examine the retention of AgNPs on the PCFs. Blank cloth and PCFs@HAC-AgNPs-1000 sheets were cut into 10 mm diameter circular pieces and sterilized under UV irradiation for 2 h. Then, subjected to washing with 20 mL of distilled water for 10 min. The effluent of these washes was collected into microtubes for antimicrobial tests, with 90 µL of each effluent and 10 µL of *S. aureus* and *B. subtilis* cultures at an OD600 (optical density at 600 nm) of 0.1. After incubating at 37°C for 18 h, serial dilutions were done, and 10 µL samples were dropped onto NA plates followed by incubation at 37°C for 18 h. Finally, the numbers of CFUs were counted.

2.10 Antibacterial activity of PCFs@HAC-AgNPs sheets

The antibacterial activity of PCFs@HAC-AgNPs sheets was assessed with *S. aureus* and *B. subtilis*. Both bacterial species were cultured overnight in an NB medium at 37°C. The optical density of the bacterial suspensions was then adjusted to an OD600 of 0.1. Then, separate sterile cotton swabs were dipped into the bacterial cultures and swabbed onto NA plates. The PCFs@HAC-AgNPs sheets were cut into 10 mm diameter circular pieces and sterilized under UV light for 2 h. Then, the AgNP sheets were placed on seeded NA plates. Finally, the NA plates were incubated at 37°C for 18 h. Zones of inhibition (ZOIs) around the disks were recorded in millimeter.

2.11 Statistical analysis

The data were displayed as mean and standard deviation (SD) values using SPSS (Version 29) software. The significance of the differences between the means of the results was assessed with one-way analysis of variance followed by Duncan's multiple range tests at a ($p < 0.05$) significance to examine the concentration effects of the AgNPs.

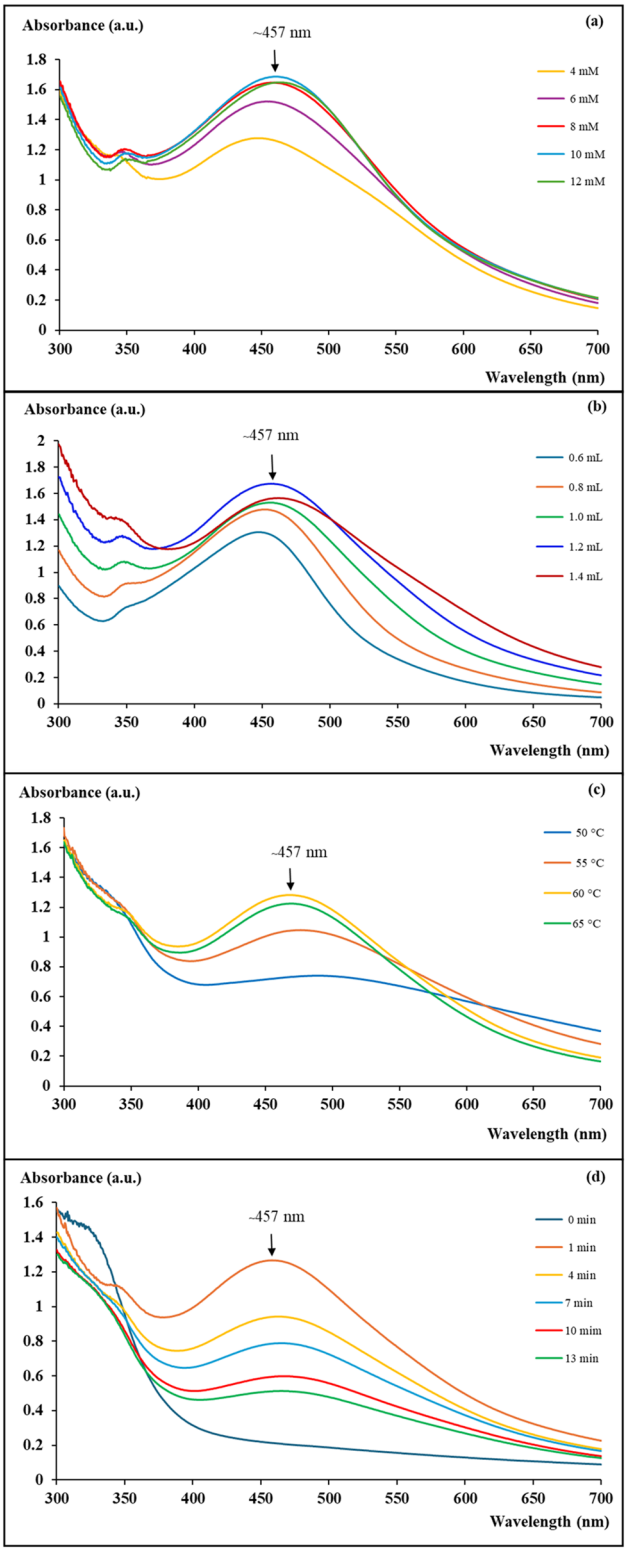

Figure 2: UV–vis spectrum of AgNP synthesis using ACLE for optimization at various (a) $AgNO_3$ concentrations, (b) volumes of ACLE, (c) temperature, and (d) time.

3 Results and discussion

3.1 Optimization of AgNP green synthesis

3.1.1 Effects of various concentrations of $AgNO_3$

Substrate concentration should be in the appropriate range due to the influence of $AgNO_3$ concentration on AgNP formation during the nucleation process. Therefore, the effects of varying $AgNO_3$ concentrations were first investigated. These results are presented in Figure 2a. The absorbance peak intensity increased gradually at $AgNO_3$ 4, 6, 8, and 10 mM concentrations. This may be attributed to increased nuclei formation resulting in the production of higher amounts of AgNPs [8]. However, a further $AgNO_3$ increase to 12 mM led to decreased absorbance peak intensity. This might have been due to excessive Ag^+ as compared to the biomolecules present in the extract. Consequently, no additional reducing agent is produced with increased $AgNO_3$ concentrations, resulting in the formation of agglomerated nanoparticles and sedimentation [22]. Therefore, a 10 mM $AgNO_3$ concentration is appropriate. This agrees with the report of Arroyo and colleagues, who found that 10 mM of $AgNO_3$ had the highest yield for AgNP synthesis with carrasquilla fruit extract (*Berberis hallii*) [23].

3.1.2 Effects of various volumes of ACLE

The concentrations of plant extracts impact the green synthesis of AgNPs by influencing the shape, size, and reduction rate of AgNPs [8]. Various volumes of ACLE were used to synthesize AgNPs (Figure 2b). Increasing the amount of ACLE resulted in a higher absorbance peak, which may be attributed to the reduction of Ag^+ ions and led to an increase in AgNP synthesis. However, when the ACLE volume was increased to 1.4 mL, the absorbance peak concentration was found to be lower, which may be due to the residual extract after the AgNPs were completely reduced. Excessive extract led to secondary layer formation, altering the electronic density of the thin layer of AgNPs, resulting in decreased absorbance peak intensity [24]. Therefore, 1.2 mL of ACLE enabled higher AgNP stability after synthesis.

3.1.3 Effects of various temperatures

Temperature may be a key factor influencing the shape and size of AgNPs. The reaction mixture was heated at

various temperatures, 50, 55, 60, and 65°C, to examine the temperature effects (Figure 2c). Absorbance peak intensity increased with reaction temperature indicating greater AgNP formation from accelerated reaction rates. At higher temperatures, molecular kinetic energy increases, promoting faster Ag^+ reaction, making particle size growth less probable. At 65°C, the absorbance peak decrease was caused by the decomposition of bioactive components coated by AgNPs or due to AgNP agglomeration [8]. Synthesis of AgNPs using ACLE at 60°C enhanced the formation of highly stable AgNPs. However, the sharpness of the absorbance peak also depends on the size of synthesized AgNPs. As the temperature increases, particle sizes will be smaller [25].

3.1.4 Effects of various reaction times

Reaction time is a factor that greatly affects the size, shape, and AgNP yield. AgNPs may agglomerate after an optimal reaction time, resulting in larger particle sizes. Figure 2d demonstrates no reduction of Ag^+ in the solution at 0 min of reaction time, as the color change of the solution was indiscernible and no AgNP absorbance peaks were observed. Formation of AgNPs was observed after a 1 min reaction and showed a higher absorbance peak intensity than for other times, indicating completion of the nucleation process. However, increased reaction time showed a significantly decreased absorption peak intensity, which might be due to diminished formation of AgNPs caused by aggregation, resulting in larger particle sizes. This leads to precipitation, making UV–vis spectroscopy difficult [8]. Therefore, the AgNP synthesis time in the current study was significantly shorter than for earlier work [12]. However, various conditionals are used for the green synthesis of AgNPs using plants as shown in Table 1.

3.2 Visual inspection

After reacting ACLE with the $AgNO_3$ solution for 2 h, the color of the solution changed from yellowish-brown to grayish-brown (inset of Figure 4a) indicating the formation of AgNPs using ACLE [30]. It is similar to the change in colors of AgNPs obtained by reference [31]. This color change is caused by the excitation of surface plasmon resonance (SPR) of AgNPs, which occurs in the collective vibrations of free electrons induced by an electromagnetic field. Electron excitation causes changes in the electronic energy level reflected in the reduction of Ag^+ to Ag^0 [12]. Wibawa and colleagues found that this phenomenon may be due to the [Kr] $4d^{10}$ (colorless) of Ag^+ transforming into [Kr] $4d^{10}5s^1$ (brown) of Ag^0. Electrons in the s orbital with a potential energy level of five lead to AgNPs that can absorb electromagnetic waves of visible light, which the human eye perceives as brown. The visible light energy excites the electron from the 5s orbital to the next 5p orbital and may be 5px, 5py, or 5pz. The energy gap formed between 5s and 5p orbitals is exactly equivalent to the quantum energy of certain visible light photons with longer wavelengths, displaying a brown color. This cannot happen with $AgNO_3$ because no electron exists in its 5s orbital, causing it to appear colorless [32]. A possible mechanism of $AgNO_3$ reduction using ACLE is shown in Figure 3. The reduction mechanism of $AgNO_3$ with polyphenols such as flavonoids from plant extracts and the hydroxyl groups (–OH) in flavonoids is crucial in reducing Ag^+. In this mechanism,

Table 1: Various conditions employed for green synthesis of AgNPs using plants

Plants	Part	Condition	Method	Size and shape	Ref.
Mikania cordata	Leaves	$AgNO_3$: 1 M	Shaking water bath	Size: 26.8–46.0 nm	[26]
			Temp: 80°C		
		Extract: 40 mL	Time: 70 min	Shape: spherical	
Vitis vinifera	Fruit	$AgNO_3$: 20 mM	Temp: room temperature	Size: 19 nm	[27]
		Extract: 10 mL	Time: 24 h	Shape: spherical	
Sambucus ebulus	Fruit	$AgNO_3$: 20 mM	Stirring	Size: 40–60 nm	[28]
		Extract: 12.5 mL	Time: 2 h	Shape: spherical	
Psidium guajava	Leaves	$AgNO_3$: 25 mM	Magnetic stirring	Size: 22 nm	[29]
		Extract: 1 mL	Temp: 60°C	Shape: spherical	
			Time: 10 min		
Ageratum conyzoides	Leaves	$AgNO_3$: 10 mM	Shaking water bath	Size: 11 nm	This work
			Temp: 60°C		
		Extract: 1.2 mL	Time: 1 min	Shape: spherical	

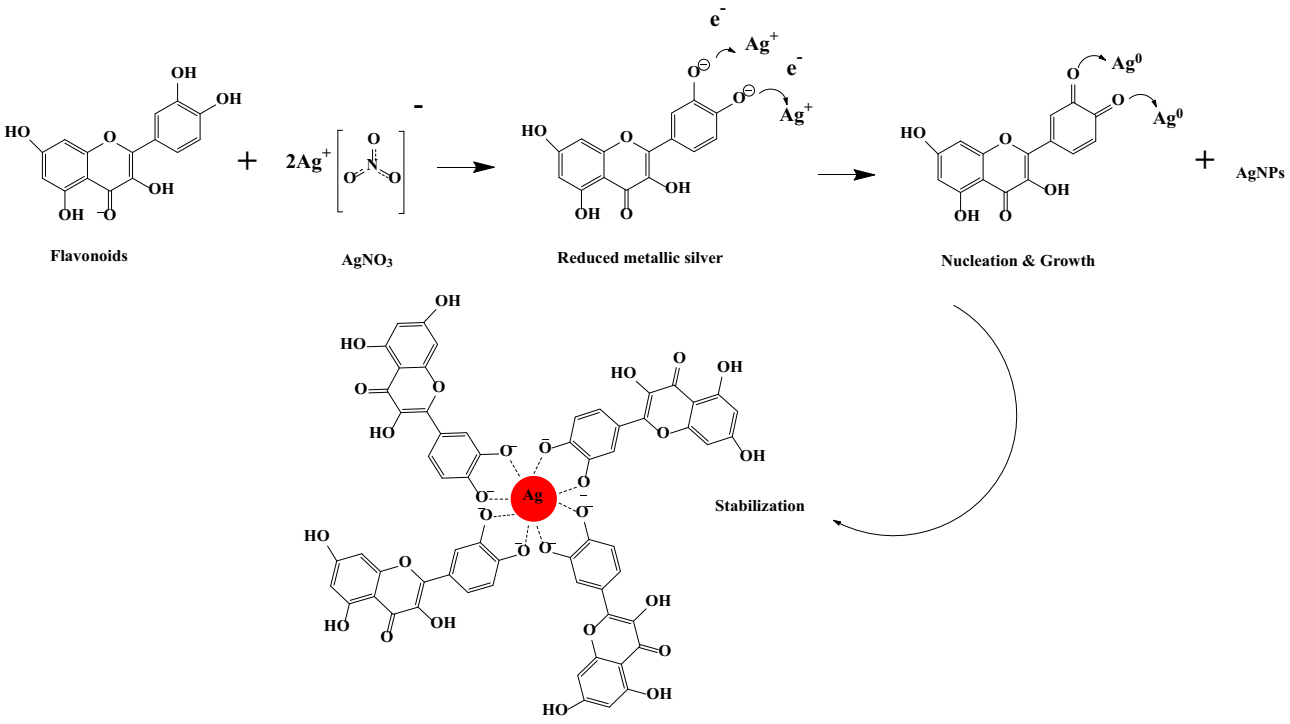

Figure 3: Schematic diagram of the possible mechanism of $AgNO_3$ reduction using ACLE.

$AgNO_3$ molecules in aqueous solution dissociate into Ag^+ and nitrate ions (NO^{3-}) when OH groups of flavonoids donate electrons to two Ag^+ ions, resulting in the reduction of Ag^+ to Ag^0 and clustering to form AgNPs [33].

3.3 Characterization of AgNPs

AgNP synthesis was also confirmed using UV–vis spectroscopy. An SRP band was observed at 457 nm (Figure 4a), which is characteristic of the plasmon absorption of AgNPs in solution, as previously reported [34]. The SPR pattern is determined by the size and shape, the dielectric properties of each type of metal particle in the synthesis medium, and adjacent inter-nanoparticle interactions. That is, the longer the SPR band, the larger the produced AgNP. Additionally, the width of the SPR band is also related to the shape of the AgNPs, with a wider range indicating the formation of non-spherical AgNPs [35]. DRS analysis was used to investigate the light absorption properties of AgNPs. The intersect of $(\alpha h\nu)^2$ versus photo energy ($h\nu$) of the tangent to this plot reasonably approximates the indirect bandgap energy. The apparent bandgap can be calculated using the Tauc plot method, as shown in the following equation:

$$(\alpha h\nu)^2 = A(h\nu - E_g) \quad (1)$$

where α is the absorption coefficient, h is Plank's constant, ν is the photon frequency, A is the absorbance, and E_g is the band gap energy. The DRS investigation of AgNPs reveals a bandgap energy of 2.16 eV (inset of Figure 4a), indicating their semiconducting characteristics. The broad energy gap from 1.3 to 2.4 eV shows properties for antibacterial, photoelectrochemical, and photocatalytic applications [36]. The morphology and particle sizes of synthesized AgNPs were investigated using FE-SEM and TEM. FE-SEM analysis showed that synthesized AgNPs were spherically shaped and homogenously distributed (Figure 4c). Moreover, the morphology and size of AgNPs were investigated under TEM (Figure 4d). This analysis showed that the AgNPs were spherically shaped with an approximate diameter of 11 nm (Figure 4b). The crystalline synthesized AgNPs were investigated with XRD. These results are shown in Figure 5. Four characteristic peaks were found at 2θ positions of 38.20, 44.46, 64.48, and 77.54°, corresponding to the (111), (200), (220), and (311) crystal planes of the face-centered cubic (fcc) structure of Ag, respectively. In addition to the characteristic XRD peaks, other peaks were observed at 2θ positions of 27.86, 32.35, and 46.34° (* marked). These peaks can be identified from the Ag_2O and AgO phases [37,38]. The presence of the oxide phases of Ag is observed when $AgNO_3$ was not completely reduced leaving residual reactant in the sample

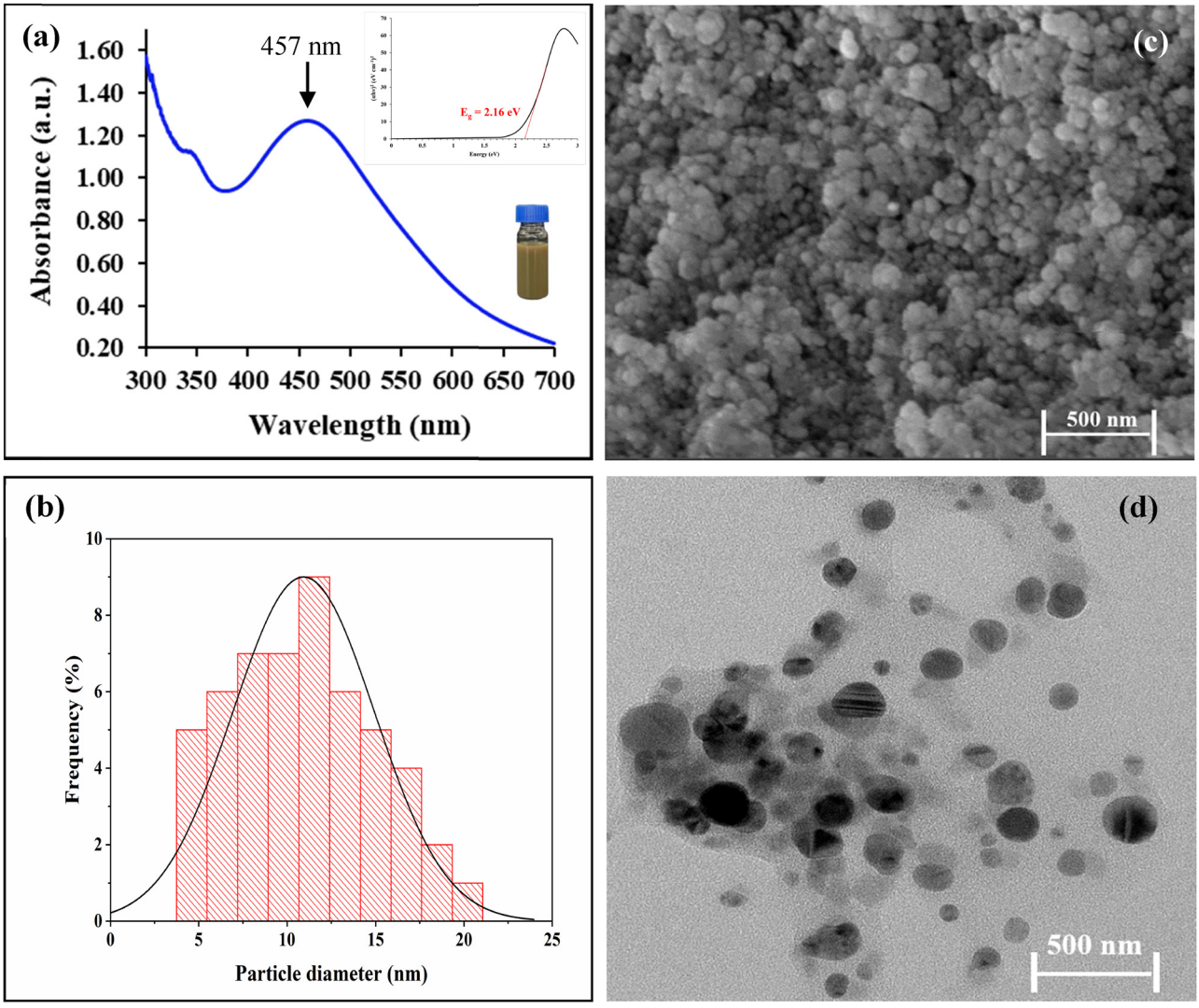

Figure 4: Characterization of the AgNP. (a) UV–vis spectrum, (b) particle size distribution, (c) FE-SEM image, and (d) TEM image of synthesized AgNPs.

[39]. Additionally, this may be due to the crystallization of organic material from the leaf extract on the surfaces of AgNPs, responsible for the reduction of Ag^+ and formation of AgNPs, which may cause AgNPs to react with oxygen in the air or the solution [29].

The surface morphology of the composite sheets before and after washing was examined using FE-SEM. This was done to confirm the adhesion and presence of HAC and AgNPs on fabric surfaces at various AgNP concentrations, as shown in Figure 6. The blank cloth (Figure 6a) had a smooth fiber surface structure with no accumulated surface particles. In Figure 6b–f, PCFs coated with HAC and AgNPs had rougher fiber surface structures caused by HAC and AgNPs. The distribution of AgNPs increased with the concentration of AgNP colloids. After 1 and 3 washing cycles (Figure 6g and h), the levels of HAC and AgNPs decreased on the fabric surfaces. The adhesion of AgNPs on the CFs was confirmed by higher magnification images and the EDS analysis shown in Figure 6i. However, plasma treatment may promote some scission in the fiber bonds, leading to OH group formation, which will increase the surface energy of the material. As a result, the material surfaces will become more hydrophilic and exhibit improved adhesion [18]. Plasma treatment of CFs before the preparation of composites increased the adhesion of AgNPs and HAC onto the CFs, which enhanced the product's effectiveness in inhibiting bacteria and increased its durability against washing.

Coating HAC and AgNPs on PCFs was further confirmed using XRD analysis. Figure 7 shows that the concentration of AgNPs-1000 coated on PCFs exhibited a distinct AgNP peak. At lower AgNP concentrations and after 1 and 3 washes, the AgNP peak was greatly diminished. This may

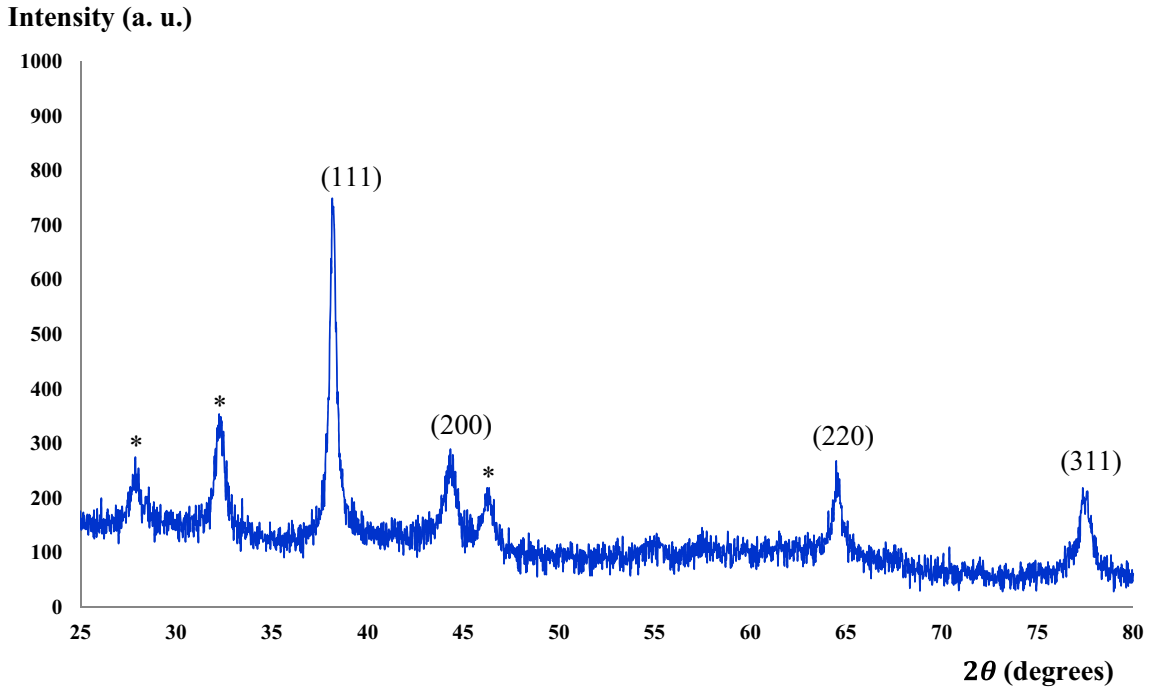

Figure 5: X-ray pattern of synthesized AgNPs.

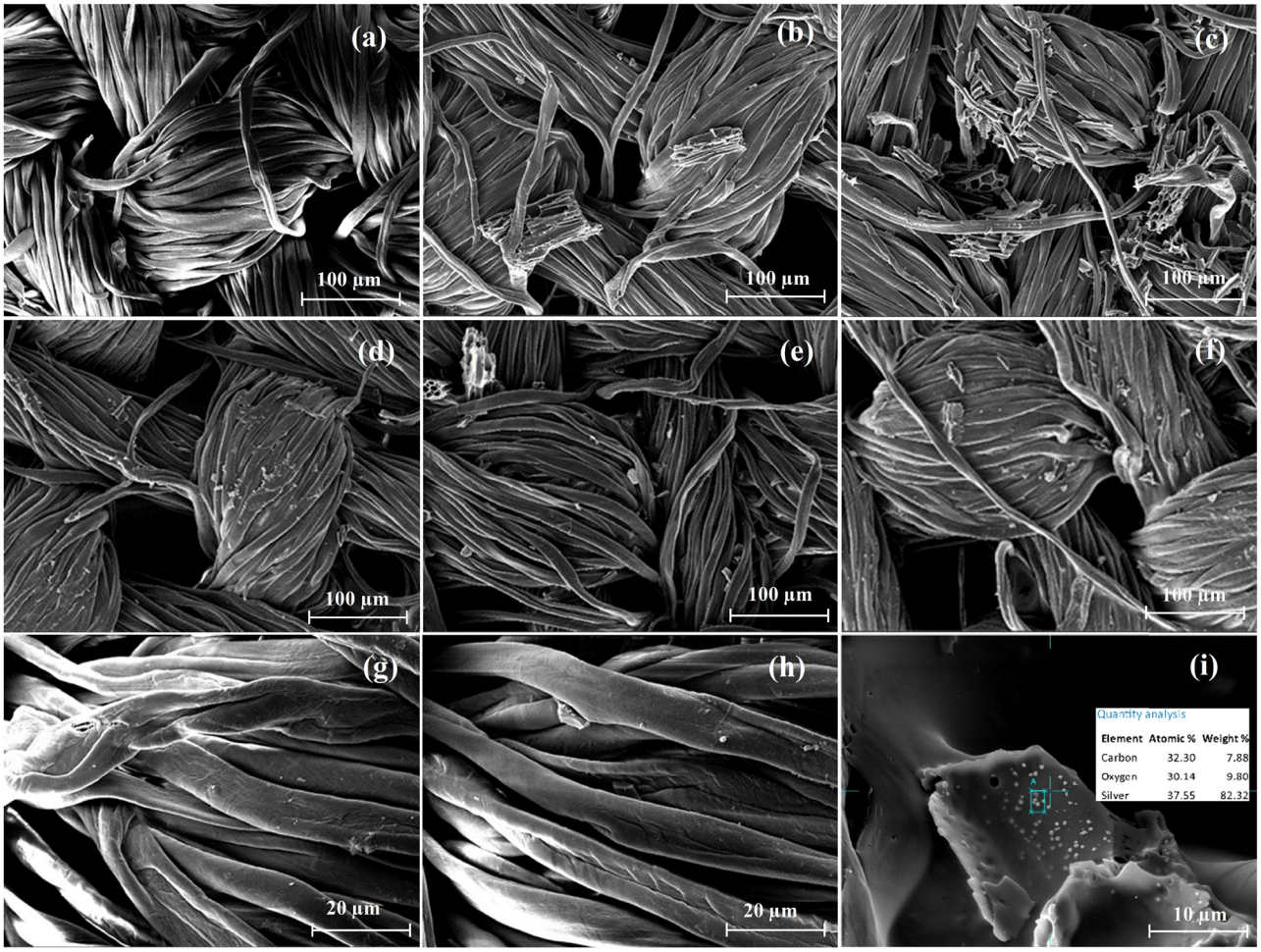

Figure 6: Surface morphology of composite sheets using FE-SEM of (a) blank cloth and AgNPs-HAC coated on PCFs before washing at various AgNP concentrations (µg/mL): (b) 62.5, (c) 125, (d) 250, (e) 500, and (f) 1,000 and the 1,000 µg/mL AgNP concentrations after washing for (g) 1 cycle, (h) 3 cycles, and (i) at high magnification and the EDS of AgNPs-HAC coated on a PCF sample.

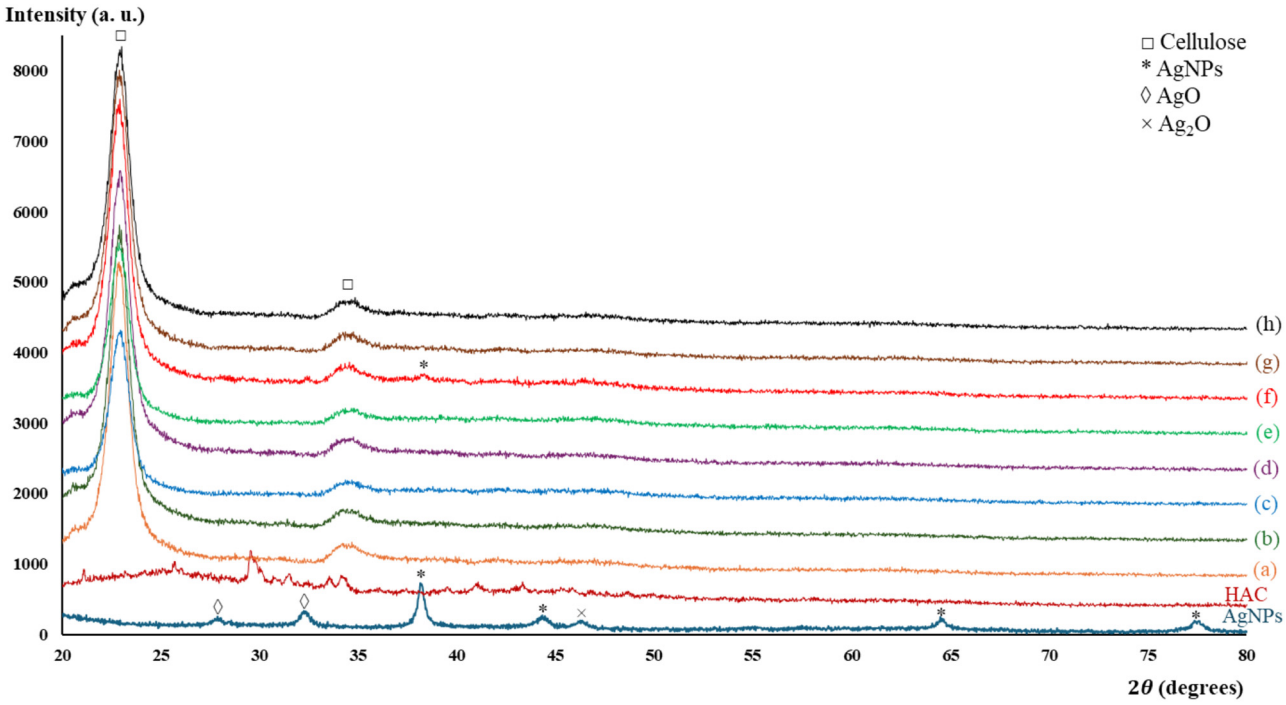

Figure 7: X-ray pattern of HAC, synthesized AgNPs, (a) blank cloth and AgNP coated cotton samples, (b) PCFs@HAC-AgNPs-62.5, (c) PCFs@HAC-AgNPs-125, (d) PCFs@HAC-AgNPs-250, (e) PCFs@HAC-AgNPs-500, (f) PCFs@HAC-AgNPs-1000, (g) PCFs@HAC-AgNPs-1000 after washing for 1 cycle, and (h) PCFs@HAC-AgNPs-1000 after washing for 3 cycles.

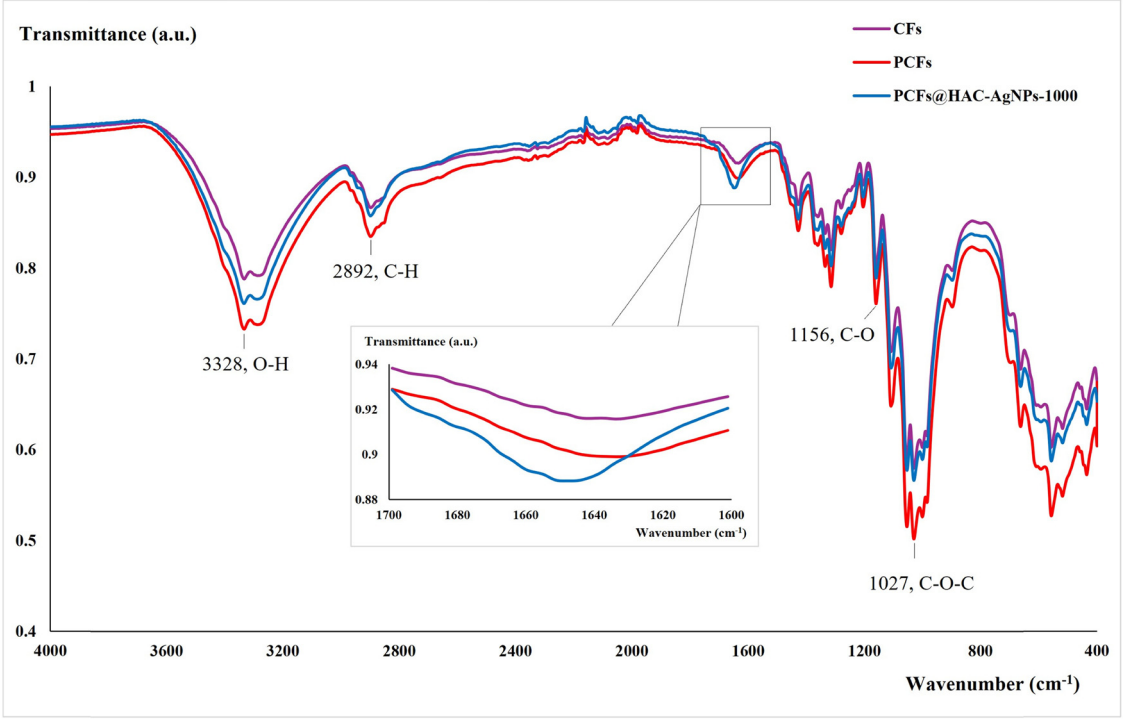

Figure 8: Fourier transform infrared spectra of CF, PCF, and PCFs@HAC-AgNPs-1000 samples.

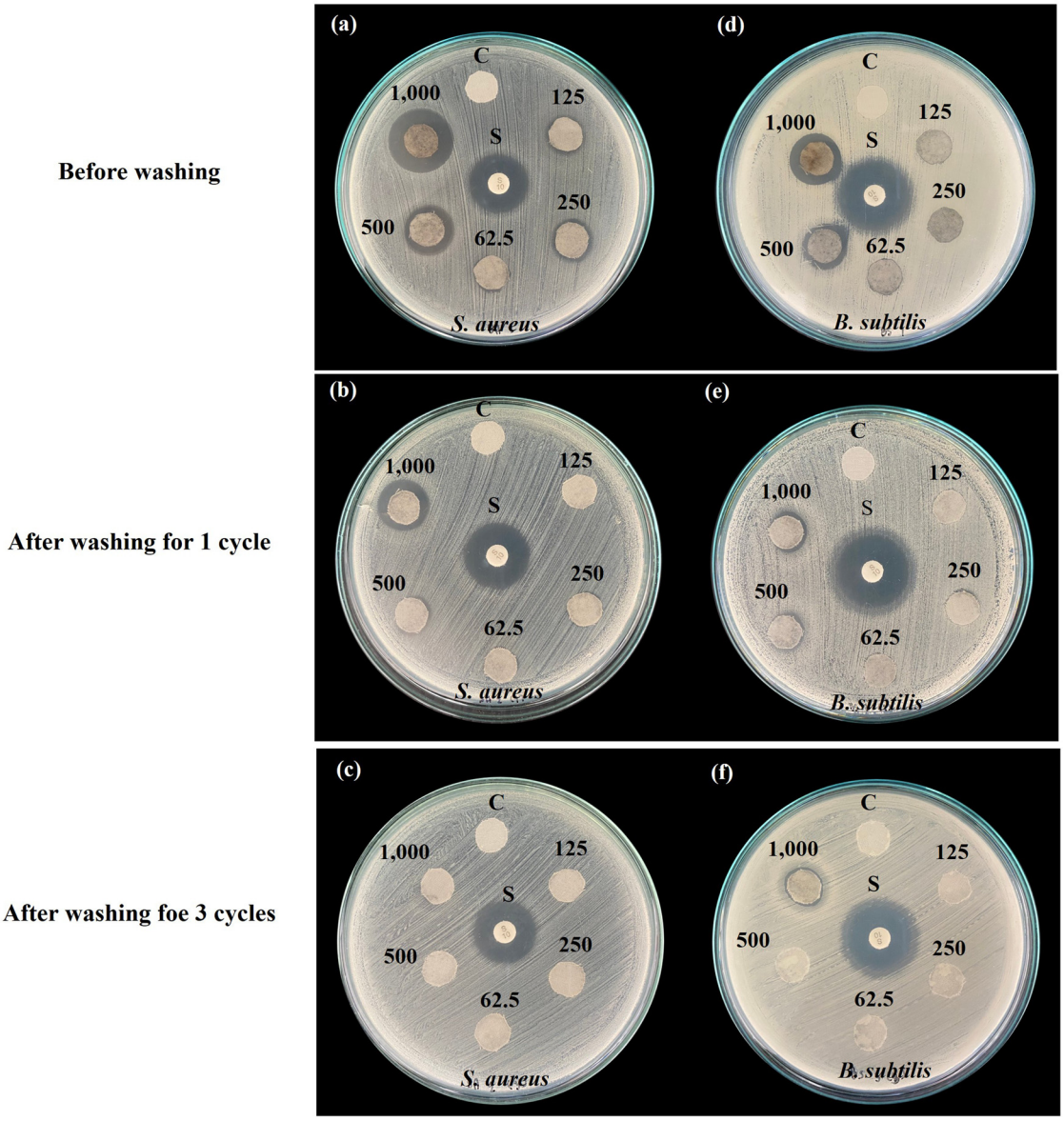

Figure 9: Antimicrobial activity of PCFs@AgNPs-HAC sheets studied using a disk diffusion method against (a–c) *S. aureus* and (d–f) *B. subtilis*, before and after washing for 1 and 3 cycles. Each panel shows different AgNP concentrations (μg/mL): 62.5, 125, 250, 500, and 1,000, C; blank cloth, and S; standard antibiotic (streptomycin).

have been due to low concentrations of AgNP colloids, HAC, and particle shedding during washing or low XRD sensitivity, resulting in a lower peak. These results indicate that HAC and AgNPs were successfully coated onto the samples, as indicated by FE-SEM imagery (Figure 6). Functional groups of CFs, PCFs, and PCFs@HAC-AgNP-1000 samples were examined under FT-IR analysis. These results are shown in Figure 8. The investigation primarily shows the characteristic peaks of the main functional groups of the CF cellulosic structure at 3,328, 2,892, and 1,156 cm^{-1}, which, respectively, correspond to O–H stretching, C–H deformation of $–CH_2–$, and C–O stretching. The major absorption peak of cotton fibers was observed at 1,645 cm^{-1}, which is caused by the vibrational deformation of molecular water absorbed by cotton fibers. The 1,027 cm^{-1} peak indicates the deformation of ether linkages (C–O–C) [40,41]. The peaks of CFs, PCFs, and PCFs@HAC-AgNPs-1000 FT-IR spectra are very similar, but the peak intensity of PCFs is greater than that of the CFs. This may be due to radical interaction with oxygen to form hydrophilic groups on the surfaces, such as –OH–, –COO–, and –CO–, caused by plasma treatment. This imparts increased surface hydrophilicity and adhesion [18]. However, no other peaks appeared indicating that no significant chemical interactions occurred

between the cellulose chains of CFs and the AgNPs, or HAC. Thus, the accumulation of AgNPs and HAC on CFs did not affect the chemical structure of the CFs. AgNPs and HAC accumulated on the fabric surfaces [41].

3.4 Antimicrobial activity evaluation of PCFs@HAC-AgNP sheets

The PCFs@HAC-AgNP sheets were evaluated for their antimicrobial activity using an agar diffusion test against foot odor-causing bacteria *S. aureus* and *B. subtilis*, both before and after laundering [42]. The sample was placed on the surface of NA medium that had been swabbed with bacteria to observe the antimicrobial activity, as shown in Figure 9. Streptomycin was used as a positive control, and untreated cloth served as a negative control. After incubation, the ZOIs around the disks were measured and recorded. The blank cloth had no inhibition zone, which indicated an absence of antibacterial activity. PCFs coated with AgNPs at 62.5, 125, 250, 500, and 1,000 µg/mL concentrations showed respective ZOI diameters of 10.83 ± 0.58, 11.50 ± 1.00, 12.50 ± 0.50, 13.83 ± 0.76, and 18.00 ± 1.00 mm for *S. aureus* (Figure 9a). *B. subtilis* showed inhibition at AgNP concentrations of 500 and 1,000 µg/mL with ZOI diameters 13.00 ± 2.00 and 14.67 ± 1.76 mm, respectively (Figure 9d). This suggests that elevated concentrations of AgNPs contribute to heightened significant bacterial inhibition as shown in Table 2 [43,44]. Although we used a high concentration of 1,000 µg/mL, the antibacterial efficacy was higher than reported by Rauf and colleagues at a concentration of 2,000 µg/mL [45]. The PCFs@HAC-AgNP sheets were subjected to laundering durability tests for one and three cycles to evaluate material reuse. These results are shown in Figure 9b–f. After one washing cycle, the AgNP 500–1,000 µg/mL concentrations still demonstrated antibacterial activity, with respective ZOI diameters of 10.83 ± 0.58 and 14.00 ± 2.18 mm for *S. aureus* (Figure 9b). ZOI diameters were 11.17 ± 0.29 and 11.67 ± 0.76 mm for *B. subtilis*, respectively (Figure 9e). Three wash cycles showed decreased bacterial inhibition. Only *B. subtilis* inhibition was seen at a 1,000 µg/mL AgNP concentration, with a ZOI diameter of 11.33 ± 0.29 mm (Figure 9f). Although PCFs@HAC-AgNP sheets underwent numerous washing cycles, their antibacterial performance remained. Alvarino and colleagues reported that AC has no antimicrobial activity. However, combining it with AgNPs significantly increased antimicrobial efficacy [46]. Bacterial inhibition by PCFs@HAC-AgNP sheets may be due to the cell wall properties of the tested bacteria. Gram-positive bacteria have a simpler cell wall structure. This allows antimicrobial compounds to more easily penetrate and reach target sites within the cells. Gram-negative bacteria have more complex cell walls that provide better resistance to antimicrobial compounds. With no cell wall, bacteria cannot withstand the environmental conditions around them and will die immediately [47]. The synthesized AgNPs are small-sized and capable of releasing silver ions (Ag^+) that penetrate bacterial cell wall pores. They can pass through the plasma membrane, lipid bilayer, and into the cytoplasm, where Ag^+ reacts with phosphorus, a component of DNA. This leads to inhibition of enzyme activity that ultimately causes bacterial cell inactivation. However, the mechanism of bacterial inhibition by

Table 2: Antimicrobial activity as zones of inhibition of PCFs@HAC-AgNPs

Test sample	Concentration (µg/mL)	Zone of inhibition (mm) ± SD	
		S. aureus	*B. subtilis*
Before washing	62.5	10.83 ± 0.58^{d}	0
	125	11.50 ± 1.00^{cd}	0
	250	12.50 ± 0.50^{c}	0
	500	13.83 ± 0.76^{b}	13 ± 2.00^{a}
	1,000	18 ± 1.00^{a}	14.67 ± 1.76^{a}
After washing for 1 cycle	62.5	0	0
	125	0	0
	250	0	0
	500	10.83 ± 0.58^{b}	11.17 ± 0.29^{a}
	1,000	14.0 ± 2.18^{a}	11.67 ± 0.76^{a}
After washing for 3 cycles	62.5	0	0
	125	0	0
	250	0	0
	500	0	0
	1,000	0	11.33 ± 0.29^{a}

Mean values with different superscripts in each row are significantly different by Duncan's multiple range test ($p < 0.05$).

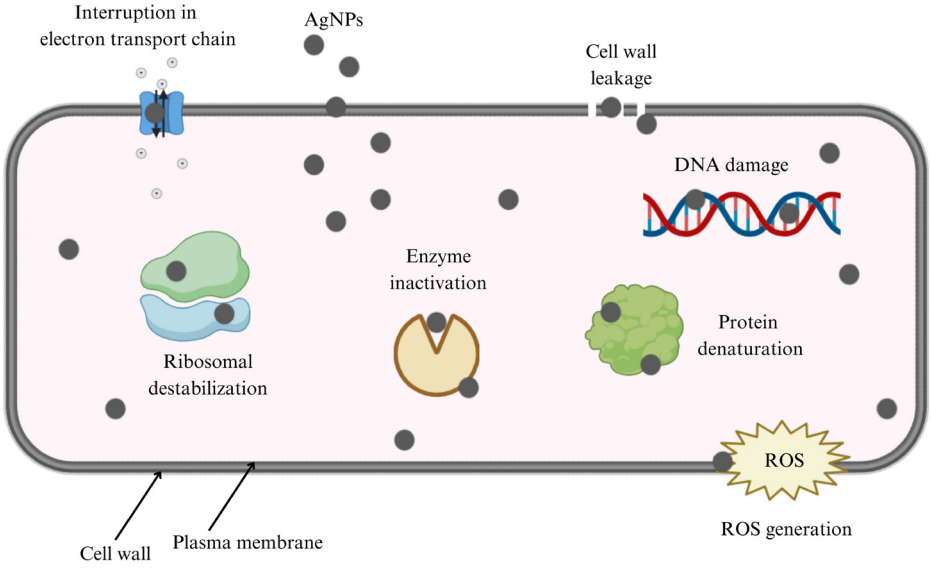

Figure 10: The mechanism of AgNP influence on bacterial cells.

AgNPs remains unclear. Multiple theories have been proposed. Small AgNPs have greater surface areas than large nanoparticles. This means that greater AgNP surface area is exposed to bacterial membranes, increasing antimicrobial activity. AgNPs can contact bacterial cell walls and cytoplasmic membranes. Positive AgNP charges interact with the negatively charged cell walls of bacteria, leading to increased cell permeability or cell leakage, which results in cell death. The interaction between AgNPs and thiol groups on the cell wall may be responsible for the generation of reactive oxygen species (ROS), causing oxidative stress, leading to enzyme and protein inhibition, destabilizing ribosomes, and interrupting the electron transport chain, and consequently, cell death [48]. The release of Ag^+ from AgNPs has a mildly acidic nature and can interact with the phosphorus and sulfur of DNA, which interrupts DNA replication, leading to cell death [33]. The proposed mechanism of AgNP influence on bacterial cells is shown in Figure 10.

Lee and colleagues evaluated skin irritation in guinea pigs and demonstrated no side effects from textiles coated with AgNPs [49]. Wen *et al.* reported that interaction between AgNPs and human fibroblasts affected their fission but was not toxic [50]. Additionally, human cells are eukaryotic, with more complex structure and functionality than prokaryotic (bacterial) cells, requiring higher concentrations of Ag^+ to cause toxicity [51].

Another problem in modifying textile surfaces with AgNPs is the fabric retention of AgNPs after washing. The effluents of a blank cloth (control) and PCFs@HAC-AgNPs-1000 sheets obtained from leaching were assessed using a drop plate method with *S. aureus* and *B. subtilis*. Our study shows that colony counts were approximately the same for cloth (8.23 log CFU/mL) and PCFs@HAC-AgNPs-1000 (8.22 log CFU/mL) for *S. aureus*, as were the counts for blank cloth (7.40 log CFU/mL) and PCFs@HAC-AgNPs-1000 (7.39 log CFU/mL) for *B. subtilis*, as depicted in Figure 11. These results show that AgNPs on PCFs have a low leaching rate. This may impact the toxicity of AgNP contamination in water, leading to health consequences [52]. However, further study is required for definitive assessment.

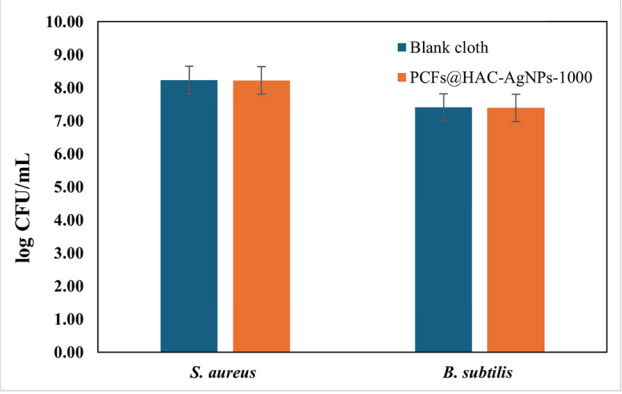

Figure 11: Antibacterial activity of effluent from washes of blank cloth and PCFs@HAC-AgNPs-1000 indicating AgNP retention on CFs.

4 Conclusions

In this study, an antibacterial material to mitigate foot odor was successfully fabricated using AgNPs and HAC coated

on PCFs (PCFs@HAC-AgNPs). AgNPs were successfully fabricated through a green synthesis from ACLE. We determined the optimum conditions for the synthesis of AgNP. They are 10 mM $AgNO_3$ and 1.2 mL of ACLE reacted at 60°C for 1 min, with incubation under dark conditions for 2 h at 30°C. AgNP synthesis was confirmed by observing the color change and measuring the absorbance peak at 457 nm under UV–vis spectroscopy. The DRS result displays an AgNP bandgap energy at 2.16 eV. FE-SEM and TEM analyses revealed that the average particle size was 11 nm. The particles were spherically shaped and homogenously distributed on fiber surfaces. Additionally, the XRD pattern shows lattice planes of the fcc structure of crystalline Ag indicating the presence of AgNPs and HAC coated on PCFs. The FT-IR pattern demonstrated that plasma technology effectively enhances the adhesion of AgNPs and HAC on PCFs without changing the internal properties of PCFs. The antibacterial activity of PCFs@HAC-AgNP sheets effectively inhibits *S. aureus* and *B. subtilis*. Furthermore, these sheets can be laundered multiple times with low environmental impact. PCFs@HAC-AgNP sheets are suitable for application as odor-reducing components of shoes.

Acknowledgments: The authors acknowledge the use of the facilities and support of the Faculty of Interdisciplinary Studies, Khon Kaen University, Nong Khai Campus. We are grateful to the faculty and staff of the Biosafety Laboratory Level II, Faculty of Interdisciplinary Studies, for their assistance.

Funding information: The authors state no funding involved.

Author contributions: All authors accept responsibility for the entire content of this manuscript and approve its submission.

Conflict of interest: The authors state no conflict of interest.

Data availability statement: All data generated or analyzed during this study are included in this published article.

References

[1] Fernández-Crehuet P, Ruiz-Villaverde R. Pitted keratolysis: An infective cause of foot odour. Can Med Assoc J. 2015;187(7):519.
[2] Yamuna V, Sudha S. Antimicrobial activity of fabrics treated with *Quercus infectoria* extract for foot odour control. BioTechnol: Indian J. 2013;7(6):231–5.
[3] Sharquie KE, Noaimi AA, Hameed SD. Topical 15% zinc sulfate solution is an effective therapy for feet odor. J Cosmet Dermatol Sci Appl. 2013;3(3):203–8.
[4] Ara K, Hama M, Akiba S, Koike K, Okisaka K, Hagura T, et al. Foot odor due to microbial metabolism and its control. Can J Microbiol. 2006;52(4):357–64.
[5] Benohanian A. Antiperspirants and deodorants. Clin Dermatol. 2001;19(4):398–405.
[6] Cherenack K, van Pieterson L. Smart textiles: Challenges and opportunities. J Appl Phys. 2012;112(9):091301.
[7] Aldana AA, Bauer J, Baker MB. Synthetic biomaterials. Tissue Engineering. 3rd edn; 2023. p. 173–212.
[8] Tesfaye M, Gonfa Y, Tadesse G, Temesgen T, Periyasamy S. Green synthesis of silver nanoparticles using *Vernonia amygdalina* plant extract and its antimicrobial activities. Heliyon. 2023;9(6):e17356.
[9] Ahmed AA, Hamzah H, Maaroof M. Analyzing formation of silver nanoparticles from the filamentous fungus *Fusarium oxysporum* and their antimicrobial activity. Turk J Biol. 2018;42(1):54–62.
[10] Hamzah H, Salah R, Maroof M. *Fusarium mangiferae* as new cell factories for producing silver nanoparticles. J Microbiol Biotechnol. 2018;28(10):1654–63.
[11] Okunade AL. *Ageratum conyzoides* L. (Asteraceae). Fitoterapia. 2002;73(1):1–16.
[12] Chandraker SK, Lal M, Shukla R. DNA-binding, antioxidant, H_2O_2 sensing and photocatalytic properties of biogenic silver nanoparticles using *Ageratum conyzoides* L. leaf extract. RSC Adv. 2019;9(41):23408–17.
[13] Selvam K, Saranya K. Phyto-mediated synthesis of silver nanoparticles using flower extract of *Erythrina indica* and evaluation of their biological activities. Inorg Chem Commun. 2023;158(2):111610.
[14] Kan CW. Evaluating antistatic performance of plasma-treated polyester. Fibers Polym. 2007;8(6):629–34.
[15] Hayashi J, Kazehaya A, Muroyama K, Watkinson AP. Preparation of activated carbon from lignin by chemical activation. Carbon. 2000;38(13):1873–8.
[16] Woskowicz E, Łożyńska M, Kowalik-Klimczak A, Kacprzyńska-Gołacka J, Osuch-Słomka E, Piasek A, et al. Plasma deposition of antimicrobial coatings based on silver and copper on polypropylene. Polimery. 2020;65(1):33–43.
[17] İşmal ÖE, Yıldırım L. Metal mordants and biomordants. The impact and prospects of green chemistry for textile technology. Cambridge: Woodhead Publishing Ltd; 2019. p. 57–82.
[18] Park Y, Koo K. The eco-friendly surface modification of textiles for deep digital textile printing by in-line atmospheric non-thermal plasma treatment. Fibers Polym. 2014;15(8):1701–7.
[19] Tooklang P, Audtarat S, Chaisen K, Thepsiri J, Chingsungnoen A, Jittabut P, et al. Functionalization of silver nanoparticles coating cotton fabrics through hydrothermal synthesis for improved antimicrobial properties. Nano Ex. 2024;5(2):025009.
[20] Chaisen K, Audtarat S, Thepsiri J, Dasri T. Development of antimicrobial cotton fabrics by decoration with silver nanoparticles and activated carbon composite. Mater Res Express. 2023;10(10):105005.
[21] Durán N, Marcato PD, De Souza GIH, Alves OL, Esposito E. Antibacterial effect of silver nanoparticles produced by fungal process on textile fabrics and their effluent treatment. J Biomed Nanotechnol. 2007;3(2):203–8.
[22] Leyu AM, Debebe SE, Bachheti A, Rawat YS, Bachheti RK. Green synthesis of gold and silver nanoparticles using invasive alien plant

Parthenium hysterophorus and their antimicrobial and antioxidant activities. Sustainability. 2023;15(12):9456.
[23] Arroyo G, Angulo Y, Debut A, Cumbal LH. Synthesis and characterization of silver nanoparticles prepared with carrasquilla fruit extract (*Berberis hallii*) and evaluation of its photocatalytic activity. Catalysts. 2021;11(10):1195.
[24] Ihsan M, Niaz A, Rahim A, Zaman MI, Arain MB, Sirajuddin S, et al. Biologically synthesized silver nanoparticle-based colorimetric sensor for the selective detection of Zn^{2+}. RSC Adv. 2015;5(111):91158–65.
[25] Mohammed Fayaz A, Balaji K, Kalaichelvan PT, Venkatesan R. Fungal based synthesis of silver nanoparticles—an effect of temperature on the size of particles. Colloids Surf B. 2009;74(1):123–6.
[26] Khatun M, Khatun Z, Karim MR, Habib MR, Rahman MH, Aziz MA. Green synthesis of silver nanoparticles using extracts of *Mikania cordata* leaves and evaluation of their antioxidant, antimicrobial and cytotoxic properties. Food Chem Adv. 2023;3:100386.
[27] Roy K, Biswas S, Banerjee PC. Green synthesis of silver nanoparticles by using grape (*Vitis vinifera*) fruit extract: characterization of the particles and study of antibacterial activity. Res J Pharm Biol Chem Sci. 2014;4(1):1271.
[28] Hashemi Z, Mizwari ZM, Mohammadi-Aghdam S, Mortazavi-Derazkola S, Ebrahimzadeh MA. Sustainable green synthesis of silver nanoparticles using *Sambucus ebulus* phenolic extract (AgNPs@SEE): Optimization and assessment of photocatalytic degradation of methyl orange and their *in vitro* antibacterial and anticancer activity. Arab J Chem. 2022;15(1):103525.
[29] Islam MJ, Khatun N, Bhuiyan RH, Sultana S, Ali Shaikh MA, Amin Bitu MN, et al. *Psidium guajava* leaf extract mediated green synthesis of silver nanoparticles and its application in antibacterial coatings. RSC Adv. 2023;13(28):19164–72.
[30] Gopu M, Kumar P, Selvankumar T, Senthilkumar B, Sudhakar C, Govarthanan M, et al. Green biomimetic silver nanoparticles utilizing the red algae *Amphiroa rigida* and its potent antibacterial, cytotoxicity and larvicidal efficiency. Bioprocess Biosyst Eng. 2021;44(2):217–23.
[31] Aritonang HF, Koleangan H, Wuntu AD. Synthesis of silver nanoparticles using aqueous extract of medicinal plants' (*Impatiens balsamina* and *Lantana camara*) fresh leaves and analysis of antimicrobial activity. Int J Microbiol. 2019;2019:1–8.
[32] Wibawa PJ, Nur M, Asy'ari M, Wijanarka W, Susanto H, Sutanto H, et al. Green synthesized silver nanoparticles immobilized on activated carbon nanoparticles: antibacterial activity enhancement study and its application on textiles fabrics. Molecules. 2021;26(13):3790.
[33] Nayem SMA, Sultana N, Haque MA, Miah B, Hasan MM, Islam T, et al. Green synthesis of gold and silver nanoparticles by using *Amorphophallus paeoniifolius* tuber extract and evaluation oftheir antibacterial activity. Molecules. 2020;25(20):4773.
[34] Hemlata, Meena PR, Singh AP, Tejavath KK. Biosynthesis of silver nanoparticles using *Cucumis prophetarum* aqueous leaf extract and their antibacterial and antiproliferative activity against cancer cell lines. ACS Omega. 2020;5(10):5520–8.
[35] Omrani AA, Taghavinia N. Photo-induced growth of silver nanoparticles using UV sensitivity of cellulose fibers. Appl Surf Sci. 2012;258(7):2373–7.
[36] Selvam K, Sudhakar C, Prasath AR. Green synthesis and characterization of silver nanoparticles from sandalwood (*Santalum album* L.) extract for efficient catalytic reduction, antioxidant and antibacterial activity. Biocatal Agric Biotechnol. 2024;57:103094.
[37] Tippayawat P, Phromviyo N, Boueroy P, Chompoosor A. Green synthesis of silver nanoparticles in aloe vera plant extract prepared by a hydrothermal method and their synergistic antibacterial activity. PeerJ. 2016;4:e2589.
[38] Liu J, Sonshine DA, Shervani S, Hurt RH. Controlled release of biologically active silver from nanosilver surfaces. ACS Nano. 2010;4(11):6903–13.
[39] Mehta BK, Chhajlani M, Shrivastava BD. Green synthesis of silver nanoparticles and their characterization by XRD. J Phys: Conf Ser. 2017;836:012050.
[40] Ahmed H, Khattab TA, Mashaly HM, El-Halwagy AA, Rehan M. Plasma activation toward multi-stimuli responsive cotton fabric via *in situ* development of polyaniline derivatives and silver nanoparticles. Cellulose. 2020;27:2913–26.
[41] Repon MR, Islam T, Sadia HT, Mikučionienė D, Hossain S, Kibria G, et al. Development of antimicrobial cotton fabric impregnating AgNPs utilizing contemporary practice. Coatings. 2021;11(11):1413.
[42] Farhamzah, Herli A, Mursal ILP. Formulation and antibacterial activity test of foot spray with Beluntas leaf ethanol extract (*Pluchea Indica* L.). IOP Conf Ser: Mater Sci Eng. 2021;1071:012013.
[43] Zahran MK, Ahmed HB, El-Rafie MH. Surface modification of cotton fabrics for antibacterial application by coating with AgNPs–alginate composite. Carbohydr Polym. 2014;108:145–52.
[44] Lavanya G, Anandaraj K, Gopu M, Selvam K, Selvankumar T, Govarthanan M, et al. Green chemistry approach for silver nanoparticles synthesis from *Halimeda macroloba* and their potential medical and environmental applications. Appl Nanosci. 2023;13:5865–75.
[45] Rauf A, Ahmad T, Khan A, Maryam, Uddin G, Ahmad B, et al. Green synthesis and biomedicinal applications of silver and gold nanoparticles functionalized with methanolic extract of *Mentha longifolia*. Artif Cells Nanomed Biotechnol. 2021;49(1):194–203.
[46] Alvarino LAdS, Manzotti F, Moreira WM, de Araújo TP, Vareschini DT, de Barros MASD. Antibacterial potential of activated carbon impregnated with garlic extract. Processes. 2023;11(10):2948.
[47] Breijyeh Z, Jubeh B, Karaman R. Resistance of gram-negative bacteria to current antibacterial agents and approaches to resolve it. Molecules. 2020;25(6):1340.
[48] Patil MP, Kim GD. Eco-friendly approach for nanoparticles synthesis and mechanism behind antibacterial activity of silver and anticancer activity of gold nanoparticles. Appl Microbiol Biotechnol. 2016;101(1):79–92.
[49] Lee HY, Park HK, Lee YM, Kim K, Park SB. A practical procedure for producing silver nanocoated fabric and its antibacterial evaluation for biomedical applications. Chem Commun. 2007;28:2959–61.
[50] Wen HC, Lin YN, Jian SR, Tseng SC, Weng MX, Liu YP, et al. Observation of growth of human fibroblasts on silver nanoparticles. J Phys: Conf Ser. 2007;61:445–9.
[51] Alt V, Bechert T, Steinrücke P, Wagener M, Seidel P, Dingeldein E, et al. An *in vitro* assessment of the antibacterial properties and cytotoxicity of nanoparticulate silver bone cement. Biomaterials. 2004;25(18):4383–91.
[52] Mat Lazim Z, Salmiati S, Marpongahtun M, Arman NZ, Mohd Haniffah MR, Azman S, et al. Distribution of silver (Ag) and silver nanoparticles (AgNPs) in aquatic environment. Water. 2023;15(7):1349.